The International Journal of Advanced Manufacturing Technology (2019) 102:3587–3596
https://doi.org/10.1007/s00170-019-03380-3

ORIGINAL ARTICLE

Effect of cryogenic cooling on adiabatic shearing in processing titanium alloy

Fengbiao Wang[1] · Yongqing Wang[2]

Received: 10 August 2018 / Accepted: 21 January 2019 / Published online: 19 February 2019

Abstract
The adiabatic shear band (ASB) is easily generated in high-speed cutting, as well as the serrated chip. The main factors are high temperature and elastoplastic instability. An adiabatic shear energy dissipation model was established and analyzed. A series of milling experiments were systematically conducted with cryogenic and conventional cooling. Meanwhile, the characteristics of the workpiece and chip were investigated and compared. The results show that under the conventional cooling, at the cutting speed of 150 m/min, the ASB and generated serrated chip can be produced with the high-frequency oscillation cutting force. In cryogenic, the chip is serrated at all kinds of cutting speed, especially high speed, and the sawtooth is regular with no obvious ASB. The serrated chip formation is mainly associated with brittle cutting in cryogenics. When the cutting parameters are unchanged, the energy dissipation is mainly determined by the main cutting force and shear strength. Compared with the conventional cooling process, the energy dissipation in cryogenic is more than the former one, and the ability of producing instantaneous adiabatic shear is weaker. Furthermore, due to the instantaneous cold brittleness of liquid nitrogen, the generating condition of the ASB is not satisfied in the shear zone.

Keywords Adiabatic shearing · Cutting parameters · Cryogenic cooling milling · Milling force · Serrated chip

1 Introduction

Because titanium alloy had a poor thermal conductivity coefficient, high specific heat, and short contact length between the chip and tool rake face [1, 2], the generated heat cannot be dissipated effectively, and the heat was mainly concentrated in a smaller range of the cutting zone and near the tool cutting edge. As a typical difficult-to-machining material, it would produce localization adiabatic shear with belt chip in low speed, small cutting depth, and large tool rake angle cutting conditions. With the constant improvement of cutting speed, the shear temperature rise stayed in a small area by moment high-speed impact between the tool and workpiece. It caused the greater softening effect than that of strain rate hardening. Meanwhile, the constitutive instability of thermal viscoplastic would have occurred, and the adiabatic shearing became inevitable with the interval adiabatic shear band (ASB) by serrated chip. This chip made the cutting process unstable and produce vibration, and it influenced the chip control, processing quality, and wearing tool [3–5]. At the same time, the adiabatic shear can cause high-frequency fluctuation of the cutting force in high-speed cutting difficult-to-machine materials. It led to increased tool wear, seriously affecting workpiece surface quality.

The important critical conditions of serrated chip formation were discussed by scholars. They generally believed that was attributed to material higher local thermal softening effect than strain strengthening and reinforcement effect of strain rate in the first deformation zone [6, 7]. But there were few scholars to focus on adiabatic shearing localization fracture which would lead to serrated chip fracture separation behavior. Komanduri [8] believed that the heat concentration in the first deformation zone resulted in the serrated chip fracture. Gente et al. [9] carried out a rapid separation test using the light-gas gun on Ti-6Al-4V, and the workpiece with the chip was obtained at the cutting speed of 2400 m/min. They also analyzed the

✉ Fengbiao Wang
wangfb@dlut.edu.cn

[1] School of Mechanical Engineering, Shenyang Ligong University, Shenyang 110159, China

[2] School of Mechanical Engineering, Dalian University of Technology, Dalian 116024, China

formation of the shear band and the expansion process of the crack. Barry [10] observed the extension of the shear zone and surface tissue of the fracture surface through the principle of cutting force pulling. Molinari [11] analyzed theoretically ASB in the titanium cutting. He found that the mechanisms of material weakening were thermal softening and material failure which was related to the accumulated plastic strain. Ren [12] investigated the effect of shock prestrain on the adiabatic shearing behavior and the dynamic mechanical properties in the cutting titanium. He obtained that the effect of shock-induced strengthening was improved at a higher reloading strain rate, and the formation, bifurcation, and interaction of ASB was accelerated. Gu [13] analyzed the influences of cutting conditions and the thermomechanical properties on the adiabatic shear fracture. The result showed that TA2 alloy was more sensitive to adiabatic shear fracture, not considering rake angle and large feed, compared with other titanium alloys.

In recent years, some scholars had conducted the cryogenic cooling process for titanium alloys. Mozammel [14] studied the cutting force and surface roughness of processing titanium alloy by cryogenic and conventional cooling through the full-factor test. It was found that the cryogenic cooling technology was better than the conventional cooling one. Lee [15] carried out the cryogenic-assisted milling process to cutting Ti-6Al-4V. And he observed the tool life was increased by 50–55% for CrTiAlN-coated tools. Park et al. [16, 17] adopted cryogenic cooling to carry out end milling titanium alloy Ti-6Al-4V with greater cutting depth. This method greatly reduced the cutting force, and the service life of tool was increased by 32% compared with the conventional cooling method. Meanwhile, it was found that the micro-lubrication method should be combined into the deep cutting process. Shokrani et al. [18] contrasted milling performances of titanium alloy in three different cooling ways including in dry cutting, cutting fluid, and liquid nitrogen. They pointed out that the surface roughness value was reduced by 30–40%, and chemical reactions between the tool and workpiece were effectively suppressed for the liquid nitrogen cooling one.

In that perspective, the adiabatic shearing was mainly caused by the plastic instability because of a quick temperature rise in the cutting zone. For our research, the liquid nitrogen inner-cooling method was used in difficult-to-machine materials, and the tool wear and serrated chip features were studied by our group [19, 20]. It was found that the serrated chip was found due to faster heat dissipation of cutting, lower temperature rise, and brittle cutting during cryogenic processing. In this paper, based on the previous achievement results, the adiabatic shear characteristics of the cryogenic cooling milling titanium alloy will be investigated deeply.

2 Prediction model of the serrated chip

2.1 Shearing deformation of the continuous chip

As shown in Fig. 1, the workpiece goes through the shear slip boundary *CD* into the shear slip region, and becomes the chip over the final line *EF*. In this region, *AB*, *CD*, and *EF* are parallel to each other, so the shear strain rate in the shear area can be considered as the average of the maximum shear strain velocity region. The mathematical relationship of strain rate, strain, stress, and temperature in the shear zone are established for the unit *Q* on *AB*. And formula (1) can be obtained.

$$\dot{\gamma}_{AB} = \dot{\gamma}_{\max} = \sqrt{\left(\frac{\partial \dot{u}}{\partial y} + \frac{\partial \dot{v}}{\partial x}\right)^2 + 4\left(\frac{\partial \dot{u}}{\partial x}\right)^2} \tag{1}$$

where $\dot{\gamma}_{AB}$ is average strain rate in *AB* and $\dot{u}$ and $\dot{v}$ are the velocities of the chip unit in *x* and *y* direction.

The speed relationship is shown in Fig. 1, which is the cutting speed v_c, the chip speed is v_p, the shear speed is v_s, and there is

$$\left.\begin{aligned} v_p &= v_c \bullet \frac{\sin\phi}{\cos(\phi-\gamma_0)} \\ v_s &= v_c \bullet \frac{\cos\phi}{\cos(\phi-\gamma_0)} \end{aligned}\right\} \tag{2}$$

where γ_0 is the tool rake angle and Φ is the shear angle. At the same time, based on the cutting theory, Φ can be expressed by

$$\phi = \arctan\left(\frac{\frac{a_p}{a_c}\cos\gamma_0}{1-\frac{a_p}{a_c}\sin\gamma_0}\right) \tag{3}$$

where a_p is cutting thickness and a_c is chip thickness.

The speed incrementing of this unit in two directions can be expressed.

$$\left.\begin{aligned} \Delta\dot{u} &= -v_s\cos\phi = -\frac{v_p\cos\gamma_0\cos\phi}{\cos(\phi-\gamma_0)} \\ \Delta\dot{v} &= v_s\sin\phi = \frac{v_p\cos\gamma_0\sin\phi}{\cos(\phi-\gamma_0)} \end{aligned}\right\} \tag{4}$$

According to the geometric relationship in Fig. 1, the length increment in *x* and *y* direction is that

$$\left.\begin{aligned} \Delta x &= \frac{h}{\sin\phi} \\ \Delta y &= \frac{h}{\cos\phi} \end{aligned}\right\} \tag{5}$$

where *h* is the shear zone thickness; it is only discussed in *x* direction in this paper.

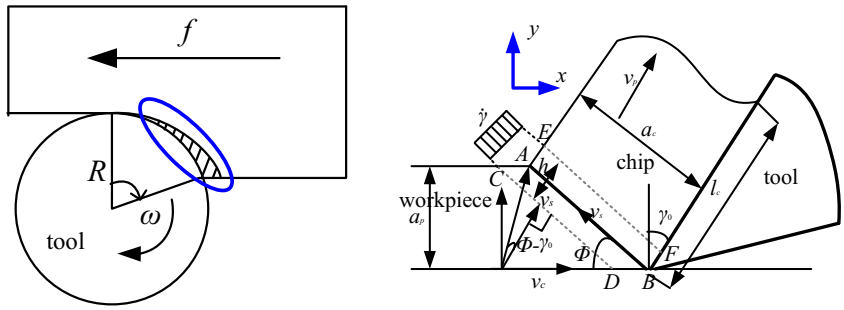

Fig. 1 Continuous chip cutting model

After the formulas (4) and (5) are substituted into formula (1), the average shear strain rate in AB is obtained by the following ones.

$$\dot{\gamma}_{AB} = \frac{v_c \cos\gamma_0}{h\cos(\phi - \gamma_0)} \tag{6}$$

The shear strain on the shear plane AB can be implied by the shear strain rate and the shear zone working time. And it has that

$$\gamma = \dot{\gamma}_{AB}\frac{\Delta x}{2v_c} = \frac{v_c\cos\gamma_0}{h\cos(\phi-\gamma_0)}\cdot\frac{h}{2v_c\sin\phi} = \frac{v_c\cos\gamma_0}{2\sin\phi\cos(\phi-\gamma_0)} \tag{7}$$

Formulas (6) and (7) show that with the increase of speed, the shear strain rate and shear strain all increase, while the energy of the shear band is going to rise. When the energy reaches the limit fracture value of localization adiabatic shearing, the serrated chip will fracture.

Also, the shear stress of rake face τ_r [21–23] can be given by

$$\tau_r = \frac{\left(F_y\cos\phi - F_x\sin\phi\right)}{\alpha_p \cdot \alpha_e} \tag{8}$$

where τ_r is the shear stress of the rake face, F_x is the cutting force in the x direction, and F_y is the cutting force in the y direction.

2.2 Adiabatic shear model

The adiabatic shear basic model based on temperature rise [21, 22] can be obtained by

$$\rho\frac{\partial v_p}{\partial t} = \frac{\partial \tau}{\partial x} \tag{9}$$

where $v_p(x, t)$ is the velocity in x long and t time, ρ is density, and $\tau(x, t)$ is the shear stress which is the same as τ_r in the rake face.

$$\frac{\partial T}{\partial t} = \frac{\tau}{\rho c}\cdot\frac{\partial v_p}{\partial x} + \xi\cdot\frac{\partial^2 T}{\partial x^2} \tag{10}$$

where $T(x, t)$ is the temperature excursion value on the shear zone. ξ is the ratio factor of cutting heat, x is cutting distance, t is working time, c is specific heat, and 0.52 J/(kg K) for Ti-6Al-4V alloy.

It was assumed that there was no heat exchange about the chip and air. By the analysis of cutting work transformation, part of the generated cutting heat was transmitted to chip, as well as another for the tool. The allocation proportion of the chip was ξ, and the tool one was $1-\xi$. Due to the same contact area temperature, the heat distribution coefficient R_ε could be expressed by formula (11) [23, 24].

$$\xi = \frac{\frac{F_y v_c A_c}{f_z\lambda_w} - T_s - T_e}{\frac{F_f v_c A_c}{f_z\lambda_w} + \frac{0.752F_f}{f_z c\rho}\sqrt{\frac{v_c}{\alpha_w\cdot l_c\cdot\omega_c}}} \tag{11}$$

where F_f is frictional force on the rake face (N); A_c is the area coefficient which is related to the ratio of the heating source length and width; λ_w is the heat conductivity coefficient (J/m s K); α_w is thermal diffusivity (m/s); it is $\alpha_w = \lambda_w/\rho c$; ω_c is the chip compress ratio; l_c is the tool-chip contact length (mm); T_s is the temperature rise caused by the shear reservoir (K); T_e is the environment temperature, the conventional of 293 K and the cryogenic of 77 K; and f_z is feed of every tooth (mm/z).

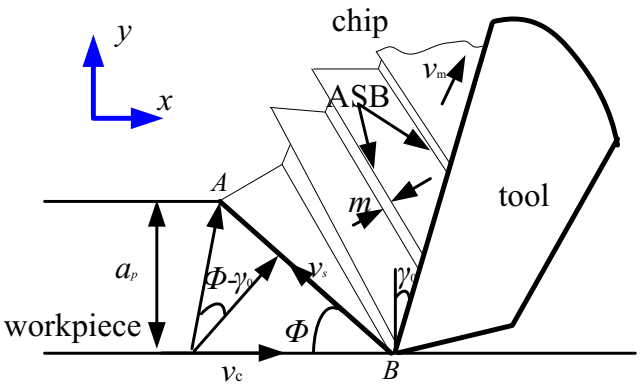

Fig. 2 Serrated chip cutting model

Table 1 Ti-6Al-4V properties in different temperature [24, 26–28]

Temperature/K	Yield strength/MPa	Tensile strength/MPa	Elasticity modulus/GPa	Shear strength/GPa	Thermal conductivity/W/(m K)
293	890	960	107	56.7	15.24
77	1420	1500	133	63.2	12.48

2.3 Serrated chip shear deformation

The forming mechanism of serrated chip is obviously different from that of strip chip. The deformation degree cannot be evaluated by the deformation coefficient. Usually, the serrated degree is as a standard to represent the chip deformation degree, and that has bigger serrated degree as well as the more sawtooth. With the study of thermoplastic constitutive relationship, the critical conditions of thermoplastic instability are studied in a large number of researches. The strain, strain rate, and temperature are considered in terms of the conditions affecting thermoplastic instability. Meanwhile, the serrated chip cutting model can be shown in Fig. 2. It is different to continuous chip cutting model (Fig. 1).

And the shear strain rate also can be expressed by

$$\dot{\gamma}_{AB} = \frac{\partial v_p}{\partial x} = \frac{v_c \cos\gamma_0}{h\cos(\phi - \gamma_0)} \tag{12}$$

For formula (10), the $\frac{\partial^2 T}{\partial x^2}$ can be estimated by formula (13).

$$\frac{\partial^2 T}{\partial x^2} \approx -\frac{\Delta T_{AB}}{2m^2} \tag{13}$$

where m is the ASB thickness and ΔT_{AB} is the cutting zone temperature rise. From the literature [25], it has that

$$\Delta T_{AB} = \frac{(1-\xi) F_s \cos\gamma_0}{\rho \cdot c \cdot a_e \cdot a_p \cos(\phi - \gamma_0)} \tag{14}$$

where ΔT_{AB} is the temperature rise and F_s is the main cutting force F_y.

Then, formula (10) can be given by

$$\frac{\partial T}{\partial t} = \frac{\tau}{\rho c} \cdot \frac{v_c \cos\gamma_0}{h\cos(\phi - \gamma_0)} - \xi \cdot \frac{\Delta T_{AB}}{2m^2} \tag{15}$$

In formula (15), ASB thickness m can be obtain from the literatures [21].

Table 2 Main elemental composition of Ti-6Al-4V wt(%)

Al	V	O	Fe	Others	Ti
5.5–6.75	3.5–4.5	0.2–0.3	≤0.5	<0.3	Allowance

$$m = \left(\frac{9\rho^3 \cdot c^2 \cdot \xi^3}{\tau^3 \cdot \dot{\gamma}} \right)^{1/4} \tag{16}$$

Adiabatic shear is associated with energy dissipation in the shear zone, as well as it has bigger energy dissipation with lower thermo-softening degree. Furthermore, the energy dissipation is mainly affected by shear thickness, material strength, the shear strain rate, and temperature increment [21, 22]. So the energy dissipated Q in the shear band can be expressed by

$$Q = m \cdot \tau \cdot \dot{\gamma}_{AB} \cdot \Delta T_{AB} \tag{17}$$

Let formulas (8), (12), (14), and (16) be substituted into formula (17); formula (18) can be obtained.

$$Q = \left(\frac{9\rho^3 \cdot c^2 \cdot \xi^3}{{\tau_r}^3 \cdot \left(\frac{v_c \cos\gamma_0}{h\cos(\phi - \gamma_0)} \right)^3} \right)^{1/4} \cdot \tau_r \cdot \frac{v_c \cos\gamma_0}{h\cos(\phi - \gamma_0)} \cdot \frac{(1-\xi) F_y \cos\gamma_0}{\rho \cdot c \cdot a_e \cdot a_p \cos(\phi - \gamma_0)} \tag{18}$$

The final formula can also be expressed after simplifying formula (18).

$$Q = (1-\xi) \cdot F_y \cdot \left(\frac{9 \cdot \tau_r \xi^3}{\rho \cdot c^2 {\alpha_p}^4 \cdot {\alpha_e}^4} \cdot \frac{v_c \cdot \cos^5\gamma_0}{h\cos(\phi - \gamma_0)^5} \right)^{1/4} \tag{19}$$

With the increase of milling speed, the material work hardening degree is improved for high toughness material. At the same time, it raises the temperature of the local shear zone and increases the material thermal softening effect. When the work hardening degree and the thermal softening effect reach equilibrium, the thermal softening will exceed the accumulated plastic work. Meanwhile, the strain hardening rate will be increased with highly localized shear deformation. As a result the adiabatic shear behavior occurred and ASB is formed.

By formulas (18) and (19), under the same cutting parameters (cutting angle, cutting force, cutting depth, cutting width, cutting speed, cutting tool angle), the energy dissipation is mainly related to the shear strength and cutting zone temperature. In conventional cooling, the shear strength is relatively

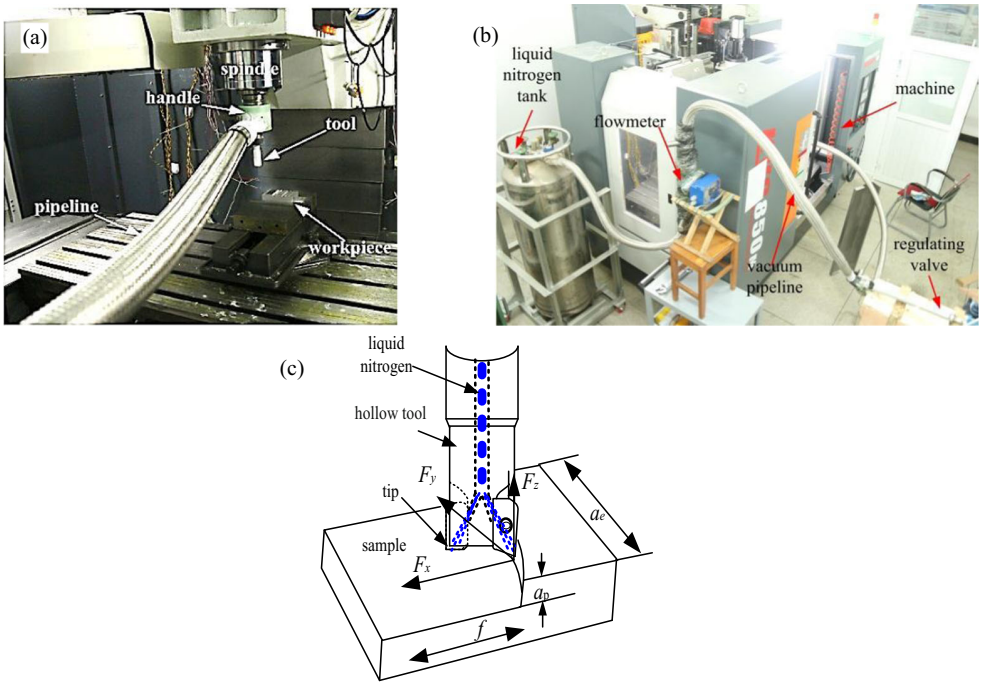

Fig. 3 Cryogenic experiment platform. **a** Experimental platform, **b** cryogenic control system, **c** milling model

Table 3 Main phases composition of the tool wt (%)

Tool brand	Phases concentration wt (%)				
	TiC	WC	Co	TaC	Others
YBG202	6	82	8	4	–

small with lower energy dissipation. At the same time, the thermal softening effect is obvious, and due to the imbalance of thermal conductivity of processed material, it has highly localized shear deformation. So the adiabatic shearing behavior will be generated, and the formation of ASB is inevitable, especially at high cutting speed. On the contrary, it has lower thermal conductivity and the higher shear strength (Table 1) with the greater energy dissipation, while the serrated chip is easy to be generated in brittle cutting of ultra-low temperature.

3 Experimental details

3.1 Experimental material

The difficult-to-machining material Ti-6Al-4V alloy used in aerospace was investigated, and its elemental components are shown in Table 2. And then it was cut into a 100 mm × 50 mm × 30 mm square piece by a wire-electrode cutting machine. After that, the surface is clean.

Table 4 Cutting parameters

No.	Cutting speed (m/min)	Cutting depth (mm)	Feed (mm/r)	Milling width (mm)	Tool nozzle temperature (K)
1	50	0.3	0.07	6	83
2	75	0.3	0.07	6	83
3	100	0.3	0.07	6	83
4	150	0.3	0.07	6	83
5	200	0.3	0.07	6	83
6	100	0.3	0.07	6	298
7	100	0.3	0.07	6	253
8	100	0.3	0.07	6	223
9	100	0.3	0.07	6	183
10	100	0.3	0.07	6	143
11	100	0.3	0.07	6	103

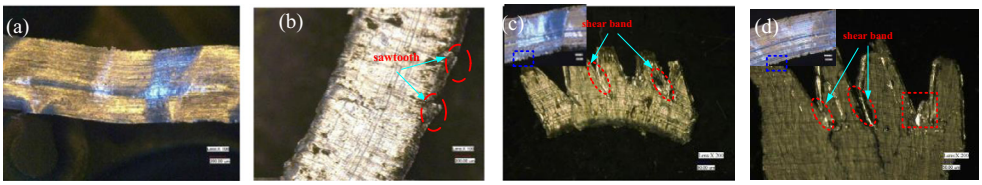

Fig. 4 Chip morphology in conventional. **a** 50 m/min, **b** 100 m/min, **c** 150 m/min, **d** 200 m/min

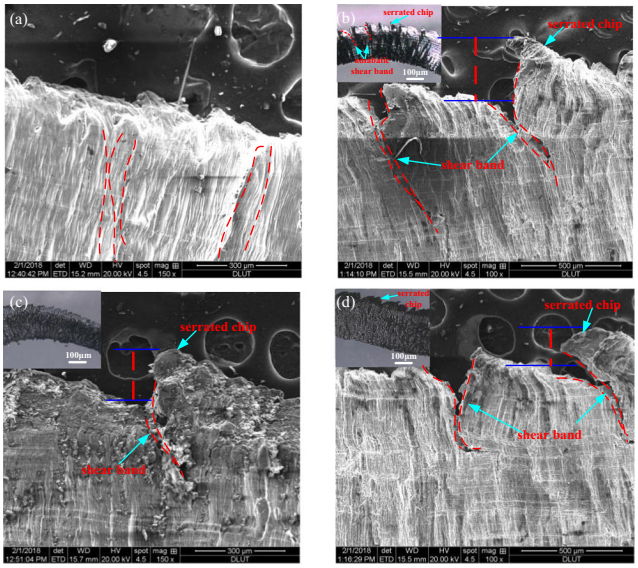

Fig. 5 SEM morphology of chip. **a** 75 m/min in conventional cooling, **b** 150 m/min in conventional cooling, **c** 50 m/min in cryogenic cooling, **d** 200 m/min in cryogenic cooling

3.2 Experimental equipment

The milling experiments were performed on a KVC850m vertical milling machining center equipped with three-axis linkage function, its highest spindle speed is 8000 r/min, and the table travel is 300 mm × 300 mm × 200 mm. The DPL - 175 MP pressurized liquid nitrogen tank was used to supply cryogenic liquid nitrogen. Within cooled handle device and control system were employed to inject liquid nitrogen with accurate flow parameters and control the liquid nitrogen nozzle temperature from 298 to 83 K. Besides Germany FUCHS water-soluble cutting fluid JM3 was used for conventional cutting.

The experiment platform and liquid nitrogen inner-cooling cutting equipment are shown in Fig. 3a, b. The hollow tool was installed in the inner-cooling handle, which was connected with the machine spindle. A blades inner-cooling vertical milling tool bar with 2 TiAlN carbide coating blades (brand for YBG202 and its phases composition were implied in Table 3) were used to processing workpieces, and its diameter of cutting department was ϕ14 mm. Considering the influence of the nitrogen phase and surface heat transfer coefficient on cryogenic machining performance in the literature [29–31], the liquid nitrogen control system was executed, which could be illuminated in Fig. 3b. According to the closed-loop feedback system included in the liquid nitrogen tank, the regulating valve, flowmeter, tool nozzle with diameterϕ0.2 mm and 0.4 MPa pressure, temperature sensors and temperature controller, and the needed nozzle temperature were set in controller. At last controlling the flow and pressure of liquid nitrogen/nitrogen mixture can reach the purpose set temperature of nozzle. Furthermore, the cutting area temperature can be measured by embedded sensors in alloy workpieces.

3.3 Experimental scheme

Using the single factor experimental method, the cutting parameters can obtained in Table 4, and they were cutting speed of $v_c = 50$, 75, 100, 150, and 200 m/min, the cutting depth of $a_p = 0.3$ mm, the feed of $f_z = 0.07$ mm/z, and the milling width of $a_e = 6$ mm, respectively. The decomposition model of the milling force is shown in Fig. 3c; there were feed force F_x, vertical force F_y named the main milling force, and back force F_z in three intersection directions. Others, a_p and a_e, were the cutting depth and the cutting width, and f_z was for the feed.

3.4 Analysis equipment

A 3D surface contour graph (ZYGO New view5022, USA) with the vertical resolution of 0.1 nm, scanning depth of 2–150 μm, and measurement of 0.001 μm was used to test surface roughness. And an ultra-deep digital microscope

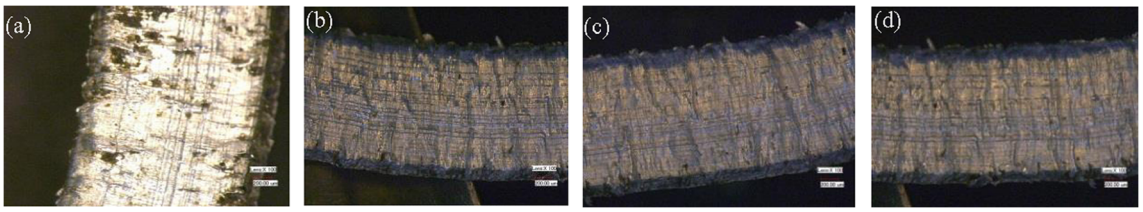

Fig. 6 Chip morphology in cryogenic. **a** 50 m/min, **b** 100 m/min, **c** 150 m/min, **d** 200 m/min

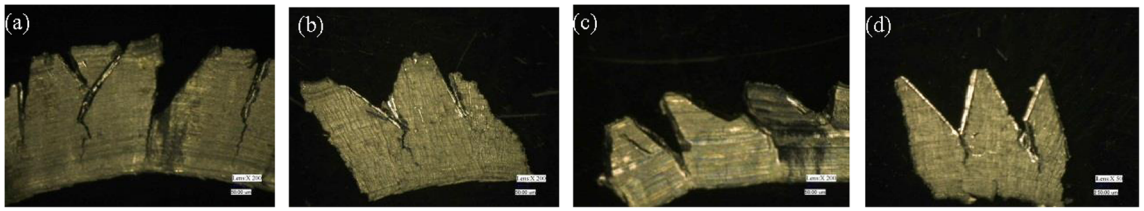

Fig. 7 Chip serrated morphology in cryogenic. **a** 50 m/min, **b** 100 m/min, **c** 150 m/min, **d** 200 m/min

(KEYENCE VHX-600, Japan) was required to measure workpiece surface morphology. Meanwhile, the milling force was measured by a three-phase dynamometer (Kisler9257B, Swiss). The surface morphology and structure were analyzed by the scanning electron microscope (SEMJSM-6360LV, Japan). The SDK TKDT 10 type contact temperature measuring instrument with the measuring range of 73–1600 K and the 0.1 K resolution was employed to measure the temperature of near blade cutting zone using the near-cutting area embedded thermocouple method.

4 Results and discussion

4.1 Chip morphology

Figure 4 shows the chip morphologies are obtained under the same cutting parameters and different cooling conditions. At low cutting speed with conventional cooling, the chip surface is basically similar to the ribbon. That is blunt and irregular on one side, and no ASB are found (Fig. 4a). With the increase of cutting speed, the serrated surface is uneven, as well as obvious locality serrated phenomenon (Fig. 4b, c). At the same time, the distribution of the serrated interval is irregular, but the serrated degree is not larger, while there was obviously a serrated chip with a non-uniform interval serrated chip at high speed (Fig. 4d). Furthermore, the adiabatic shearing bands are more obviously at higher cutting speed from 150 m/min to 200 m/min, as illuminated in the elliptical regions in Fig. 4c, d. Meanwhile, the serrated depth increases and the serrated pattern has deviation and stripped phenomenon (square region in Fig. 4d).

As well as in conventional cooling, the organization of the chip has the squeezed traces (shown dotted lines in in Fig. 5a). Similarly, there was an obvious serrated chip as the speed is up to 150 m/min, and that can form ASB, as shown in Fig. 5b. But the serrated chip is irregular, and the height and width have all a big change grads.

In cryogenic, it is not obvious difference for chip morphology at low and middle speeds (Fig. 6a, b), and the brittle cutting plays a leading role [20]. The increase of cutting speed does not lead to the obvious tissue changes in the serrated chip. That is to say the grain is not elongated and broken in the shear direction. As illuminated in Fig. 6c, d, the temperature is still lower in the shear zone even at the higher speed. Phenomenon of organization dynamic recrystallization and refine are not appeared under the instantaneous cryogenic cooling, Organization transformation of cold quenching is difficultly formed, only part of the titanium alloy organization has the phase transformation in cryogenic. Furthermore, although there has been a serrated chip at every speed, the ASB cannot almost be found in the speed between 50 and 200 m/min (Fig. 5c, d), and the sawtooth is regular.

As illuminated in Fig. 7, there are all serrated structures at cutting speed from 50 to 200 m/min through the chip serrated morphology in cryogenic (Fig. 7a, b). But the ASB cannot

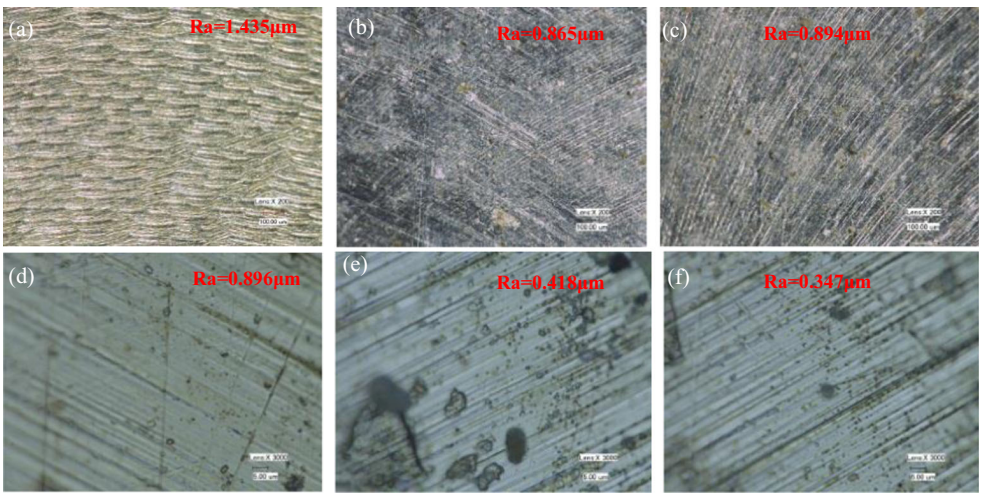

Fig. 8 Surface morphology of processed workpiece. **a** 75 m/min in conventional, **b** 150 m/min in conventional, **c** 200 m/min in conventional, **d** 75 m/min in cryogenic, **e** 150 m/min in cryogenic, **f** 200 m/min in cryogenic

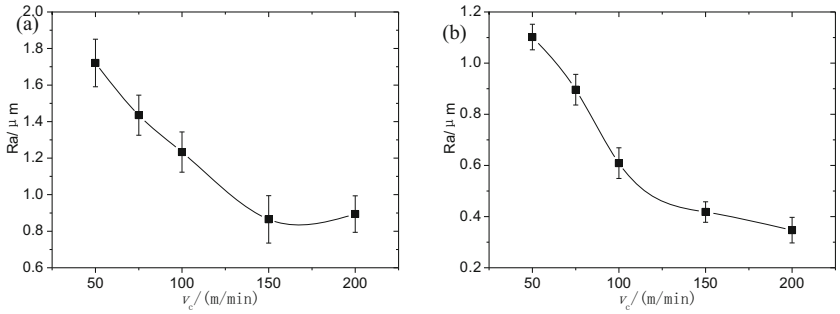

Fig. 9 Surface roughness. **a** Conventional cooling processing, **b** cryogenic cooling processing

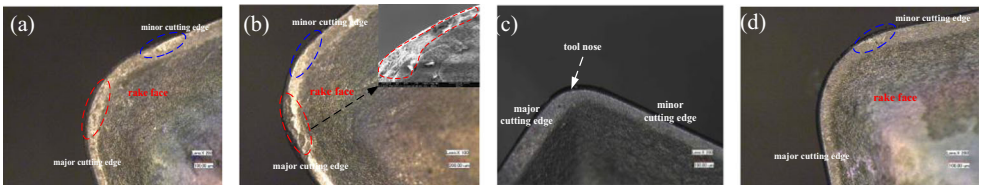

Fig. 10 Tool morphology. **a** 75 m/min in conventional cooling, **b** 150 m/min in conventional cooling, **c** 75 m/min in cryogenic cooling, **d** 200 m/min in cryogenic cooling.

also be identified, and only the crack is seen in the serrated intervals. Especially the crack is obvious and the serrated structure is regular at higher speed (Fig. 7c, d).

Chip morphology reflects the deformation degree in the machining process. The toughness of processed material plays a leading role in the conventional cooling cutting. It implies that has the strong plastic deformation in serrated chip material. The main reason is that it is easy to produce titanium alloy serrated chip with high frequency oscillation of cutting force at high-speed cutting. It causes local uneven force between workpiece and tool. Under the combined action of strain and heat, thermal (viscous) plastic instability is produced. Meanwhile, the microstructure hardness and thermal conductivity of workpiece material are not evenly distributed. It causes the uneven plastic deformation in processing. And the dislocation slip is formed in the deformation time and space in the same position. Furthermore, the deformation bands transform to the phase ones in the shear zone.

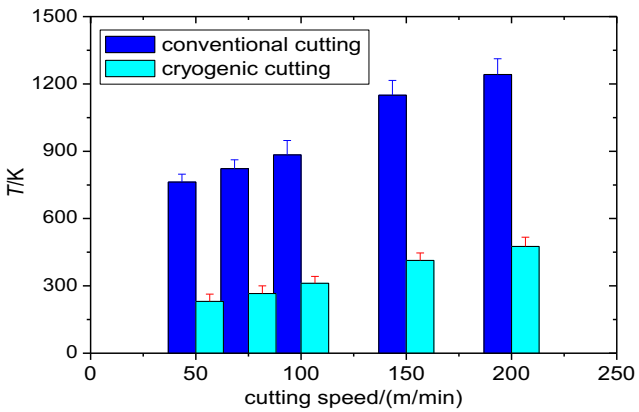

Fig. 11 Influence of cutting speed on temperature

4.2 Processed surface roughness

The thermal conductivity of titanium alloy is lower, and the cutting temperature is lower at low cutting speed (75 m/min), as shown in Fig. 8a. The plastic deformation plays a major influence to surface roughness. With the increase of speed, the plastic deformation time becomes shorter and the deformation degree is smaller, so the surface roughness decreases (Fig. 9a). When the speed reaches a certain scope (between 150 and 200 m/min), the cutting temperature rises sharply. Then, the material thermal softening effect plays a leading role, and adiabatic shearing occurs. Similarly, the high-frequency vibration in the tool nose can be found, and the tool rake worn seriously, especially the major cutting edge, as seen in Fig. 10a, b. That seriously influences processing surface quality, while the roughness value increases instead (Fig. 8b, c and Fig. 9a).

However, in the condition of cryogenic cooling, the surface roughness always decreases with cutting speed, and the surface quality is improved, as illuminated in Fig. 8d–f and Fig. 9b. At a higher speed, this change trend slows down. It can be deduced that the thermal softening effect is not obvious, and the high-frequency vibration is weakened. Although it has a higher cutting speed (200 m/min), the tool wear is still slight, and it can be obtained by Fig. 10c, d. Furthermore, it also can be implied that the wear is improved between the flank surface and the processed surface.

4.3 Cutting temperature

As illuminated in Fig. 11, the cutting temperature is higher in conventional cooling, and it is over 1200 K at 200 m/min. The wear between tool and chip is very acute with cutting speed.

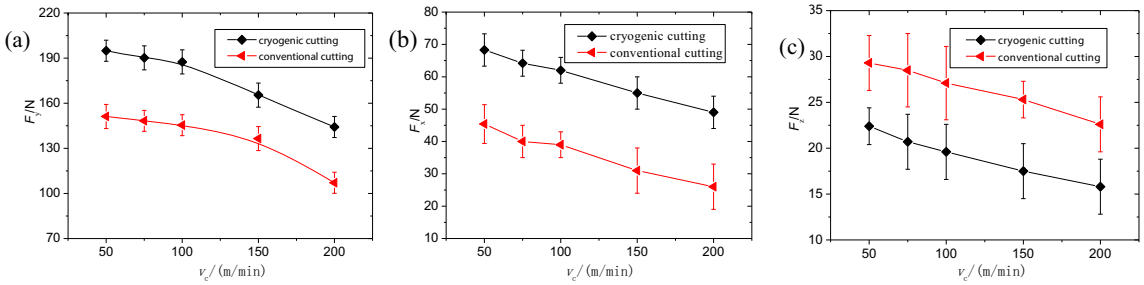

Fig. 12 Effect of cutting speed on milling force. **a** Main cutting force, **b** feed force, **c** back force

At the same time, it must produce a lot of friction heat. But titanium alloy has poor thermal conductivity, and the cutting heat cannot be taken away by the chip soon and gathered in the cutting zone. Although the cutting liquid can play a cooling role, the temperature is still rising rapidly. This makes the adiabatic shearing serious. But in cryogenic conditions, the temperature is much lower than the former one, and it is slow growth with speed change. It explains that liquid nitrogen is better to improve significantly cooling effect than conventional cutting liquid while it promotes energy dissipation of the cutting zone. Furthermore, the temperature of the cutting zone is only 450 K at 200 m/min, and it is significant less than the conventional one. So that has a bigger value considering the energy dissipation model. So the low temperature obviously can inhibit adiabatic shear conditions. Furthermore, the material has embrittlement phenomenon in cryogenic cutting, and the serrated degree increases with more uniform sawtooth, especially at high speed.

4.4 Cutting force

In the process of cutting Ti-6Al-4V, the degree of adiabatic shearing depends not only on the performance of the cutting tool and workpiece material but also on the cutting temperature. Meanwhile, the high pressure makes the contact surface produce large plastic deformation in the contact area. Similarly, the greater change of the cutting force leads to the tool continuously bearing alternating load with a great serration chip. The load will severely destroy the tool.

Near the tool cutting edge, besides the high cutting temperature, the cutting force is also high, as shown in Fig. 12, especially the main one F_y (Fig. 12a) and the feed force F_x (Fig. 12b). This is mainly due to the lower elastic modulus of titanium alloy, which leads to larger processing rebound. The rebound causes more violent friction between the rake face and cutting surface. That is the most important factor of adiabatic shearing. But the elastic modulus is relatively larger in cryogenic. Therefore, the rebound degree is small and serrated degree is also light and regular.

It can be seen from formula (7) in Section 2.1 that the shear strength is increased with the increase of cutting force. At the same cutting speed, the cutting force in cryogenic cooling is larger than that of conventional ones, and the shear strength is larger, which corresponds to Table 1. So it can be seen from formula (19) that the energy dissipation is large in cryogenic, while the F_z (Fig. 12c) is lower which can deduce that the rebound and vibration are also less. So the adiabatic shear is small and regular, especially at high speed. Furthermore, the chip is mainly generated by brittle cutting in cryogenic [19].

5 Conclusions

In this paper, the research result of the adiabatic shear with a serrated chip for milling Ti-6Al-4V alloy in conventional and cryogenic is reported. The following conclusions can be rigorously claimed.

(1) At the cutting speed of 150 m/min with conventional cooling, it begins to generate ASB and non-uniform serrated chip with high-frequency oscillation cutting force. More than this speed, the surface quality of the processed workpiece is affected, and the stick and plastic finstability can be deduced under the action of strain and high temperature.
(2) Compared with conventional cooling, the chip is serrated especially high speed at all kinds of cutting speed with the cryogenic cooling process. At the same time, the sawtooth is regular, and it is no obvious ASB. The formation of the serrated chip is mainly associated with brittle cutting in cryogenic.
(3) Furthermore, based on the established adiabatic shear energy dissipation model, when the cutting parameters were unchanged, the energy dissipation was mainly determined by the main cutting force and shear strength. Compared with conventional cooling, these factor values are all bigger in the cryogenic condition with bigger energy dissipation in cryogenic cooling. So the ability of producing instantaneous adiabatic shear is weaker. As well as due to the instantaneous cold brittleness of liquid nitrogen, the generating condition of ASB is not satisfied in shear zone, so ASB is not easy to be generated.

Acknowledgements This research was partially supported by the natural science foundation project of Liaoning province (No. 20170540787), the Liaoning key fund of national natural science fund (No. U1608251), and the basic science and research project of Liaoning province (No. LG201711).

References

1. Alborz S, Vimal D, Stephen TN (2016) Investigation of the effects of cryogenic machining on surface integrity in CNC end milling of Ti–6Al–4V titanium alloy. J Manuf Process 21:172–179
2. Raza S W, Pervaiz S, Deiab I(2014) Tool wear patterns when turning of titanium alloy using sustainable lubrication strategies 15(9): 1979–1985
3. Ye GG, Xue SF, Ma W, Jiang MQ, Ling Z, Tong XH, Dai LH (2012) Cutting AISI 1045 steel at very high speeds. Int J Mach Tool Manu 56:1–9
4. Xie J, Bayoumi A, Zbib H (1998) FEA modeling and simulation of shear localized chip formation in metal cutting. Int J Mach Tool Manu 8:1067–1087
5. Wang BF, Li J, Sun JY (2014) Adiabatic shear bands in Ti-6Al-4V alloy with lamellar microstructure. J Mater Eng Perform 23(5): 1896–1903
6. Hou Z, Komanduri R (1997) Modeling of thermomechanical shear instability in machining. Int J Mech Sci 39(11):1273–1275
7. Li GH, Wang MJ, Duan CZ (2009) Adiabatic shear critical condition in the high-speed cutting. J Mater Process Technol 209(3): 1362–1367
8. Komanduri R, Schroeder T (1986) On shear instability in machining a nickel-iron base superalloy. J Eng Ind Trans ASME 108(2):93–100
9. Gente A, Hoffmeister H, Evans C (2001) Chip formation in machining Ti-6Al-4V at extremely high cutting speeds. CIRP Ann Manuf Technol 50(1):49–52
10. Barry J, Byrne G (2002) The mechanisms of chip formation in machining hardened steels. J Manu Sci Eng 124(3):528–535
11. Molinari A, Soldani X, Miguelez MH (2013) Adiabatic shear banding and scaling laws in chip formation with application to cutting of Ti-6Al-4V. J Mech Phys Solids 61(11):2331–2359
12. Ren Y, Yu XD, Tan CW, Li XS (2019) Dynamic mechanical properties and adiabatic shearing behavior of the shock prestrained Ti-6Al-4V alloy having bimodal microstructure. J Alloys Compd 773: 1054–1063
13. Gu LY (2018) Critical condition prediction of adiabatic shear fracture in high-speed cutting TA2 alloy. Int J Adv Manuf Technol 94(5-8):2981–2991
14. Mozammel M (2017) Multi-response optimization of end milling parameters under through-tool cryogenic cooling condition. Measurement 111:134–145
15. Lee I, Bajpai V, Moon S, Byun J, Lee Y, Park HW (2015) Tool life improvement in cryogenic cooled milling of the preheated Ti–6Al–4V. Int J Adv Manuf Technol 79:665–673
16. Park KH, Suhaimi MA, Yang GD (2017) Milling of titanium alloy with cryogenic cooling and minimum quantity lubrication (MQL). Int J Precis Eng Manuf 18(1):5–14
17. Park KH, Yang GD, Suhaimi MA (2015) The effect of cryogenic cooling and minimum quantity lubrication on end milling of titanium alloy Ti-6Al-4V. J Mech Sci Technol 29(12):5121–5126
18. Shokrani A, Dhokia V, Newman ST (2016) Comparative investigation on using cryogenic machining in CNC milling of Ti-6Al-4V titanium alloy. Mach Sci Technol 20(3):475–494
19. Wang FB, Liu JK, Shu QL (2017) Milling wear of carbide tool for processing nickel-based alloy in cryogenic based on the entropy change. Int J Adv Manuf Technol 90:1703–1713
20. Wang FB, Liu JK, Shu QL (2017) Research on tool wear of milling nickel-based superalloy in cryogenic. Int J Adv Manuf Technol 91: 3877–3886
21. Grady DE (1992) Properties of an adiabatic shear band process zone. J Mech Phys Solids 40(6):1197–1215
22. Grady DE (2017) Physics of shock and impact. IOP Publishing, Bristol, pp 131–204
23. Jiang J, Li YQ, Zhang ZY (1991) Manufacturing technology of titanium alloy parts. National Defence Industry Press, Beijing, pp 25–101
24. Wang J Y, Ge Z M (1985) Aviation titanium alloy. Shanghai Science and Technology Press, Shanghai.pp:31–98
25. Oxlev PLB (1989) Mechanics of machining: an analytical approach to assessing machinability. Halsted Press, Chichester, pp 100–176
26. Bang J, Byrne G, Lennon D (2001) Observations on chip formation and acoustic emission in machining Ti-6A1-4V alloy. Int J Mach Tool Manu 41:1055–1070
27. Ginting A, Nouari M (2009) Surface integrity of dry machined titanium alloys. Int J Mach Tool Manu 49(3–4):325–332
28. Cotterell M, Byrne G (2008) Dynamics of chip formation during orthogonal cutting of titanium alloy Ti-6A1-4V. CIRP Ann Manuf Technol 57:93–96
29. Huang XD, Zhang XM, Mou HK et al (2014) The influence of cryogenic cooling on milling stability. J Mater Process Technol 214:3169–3178
30. Ravi S, Pradeep Kumar M (2011) Experimental investigations on cryogenic cooling by liquid nitrogen in the end milling of hardened steel. Cryogenics 51:509–515
31. Sharm VS, Dogra M, Suri NM (2009) Cooling techniques for improved productivity in turning. Int J Mach Tool Manu 49:435–453